Chapter 3

GRADUAL EMERGENCE OF ORDERING IN THE SPIN-FRUSTRATED $Dy_2Ti_{2-x}Mn_xO_7$

3.1 Introduction

In a pioneering paper [78], Griffiths investigated a percolation transition in an Ising ferromagnet and showed that a new phase consisting of ferromagnetic clusters within the paramagnetic matrix observed above the Curie temperature. This phase regime is called the Griffiths phase (GP) [79]. The nucleation of finite-sized correlated regions or clusters with short-range magnetic ordering within a global paramagnetic matrix occurring above the magnetic transition temperature leads to the formation of this phase. An experimental observation of GP was made by Salamon et al. using magnetic susceptibility measurements on a hole-doped manganite system [80].

It is, therefore, possible to probe the Griffiths phase by measuring the temperature variation of magnetic susceptibility at different fields. "The temperature-dependent inverse susceptibility curves, i.e. χ^{-1} (T)" show a downturn behaviour in the Griffiths phase regime, which is a "hallmark" for identifying the Griffiths phase. It should be noted that observing χ^{-1} (T) down-turn behaviour at low fields is extremely important since it eventually enables one to distinguish the GP from other non-Griffiths, such as clustered phases, where χ^{-1} (T) deviates from Curie-Weiss (CW) rule by exhibiting an up-turn above ordering temperature. It is

observed that the downturn behaviour softens with increasing magnetic field strength, and with sufficiently high magnetic field strength, CW-like behavior is observed, which is also characteristic of GP. Since magnetization increases linearly with magnetic field in paramagnetic regions, PM susceptibility predominates over the correlated clusters' contribution to susceptibility at high fields. GP regime does not follow CW law; rather, it follows the power law of inverse susceptibility. During the initial studies, it was believed that only a ferromagnetic system is a prerequisite for the exhibition of Griffiths's phase. However, recently, a few reports have observed Griffiths's phase in some antiferromagnets as well [81], [82].

In the present study, it has been observed that a small magnetic disorder at the B site gives rise to the emergence of a GP-like phenomenon. We have substituted magnetic Mn at the Ti site in the $Dy_2Ti_2O_7$ matrix, i.e., $Dy_2Ti_{2-x}Mn_xO_7$. We have used dc and ac magnetic susceptibility to investigate the nature of this magnetic interaction in the doped spin ice. Both the spin relaxations of the thermal and quantum regimes have been investigated. The system remarkably exhibits a spectrum of competing magnetic phases between 12 K to 4 K. It has been shown that spin ice freezing temperature shifts to a higher temperature with Mn inclusion, and a new peak (T*) emerges between T_i and T_s at around 5 K. The new peak can be attributed to GP-like due to the formation of magnetic clusters having short-range magnetic ordering, as verified by magnetic studies. Dy-Mn spins interaction and altered crystal fields play an important role in determining the magnetic state of this disordered compound. This suggests that a relatively low level of Mn inclusion at the Ti site changes the number and type of relaxation processes available to the spins, making it an exciting system to study its low-temperature spin dynamics. This chapter presents structural analysis and detailed magnetic

studies using ac susceptibility, M-T, and M-H measurements for Mn-substituted Ising type pyrochlore.

3.2 Structural Analysis

The polycrystalline $Dy_2Ti_{2-x}Mn_xO_7$ (x=0, 0.05, 0.10, 0.15, 0.20) samples were prepared using the conventional solid-state reaction method. $Dy_2Ti_2O_7$ exhibits cubic pyrochlore structure with space group $Fd\bar{3}m$ and unit cell comprise 8 formula units, i.e., 88 atoms per unit cell. $Dy_2Ti_2O1_6O2$ is the preferable formula, and the O1 oxygen atom forms anti-prismatic arrangement around the central Dy ion. The crystal-field environment of a Dy^{3+}ion in a magnetic pyrochlore oxide is such that the edges of the triangles connect six coplanar oxygens (say, O1): three above and three below the plane of the Dy^{3+} and Ti^{4+} ions. It will result in two parallel planes containing the respective triangles of O1 ions. The plane is transverse to the O2-Dy-O2 linear axis. A strong axial symmetry is exhibited along the [111] axis, which is the direction containing two O2 atoms connected through the shared Dy^{3+} atom of the adjacent tetrahedra. The two oxygen ions (say, O2 ions) are aligned along the [111] axis with the central Dy^{3+} is responsible for the local Ising anisotropy. The Ti^{4+} ions are arranged in a hexagon coplanar with the Dy^{3+} ion in the center [83], [84].

High-resolution x-ray diffraction (HRXRD) pattern of $Dy_2Ti_{2-x}Mn_xO_7$ (x = 0.00, 0.05, 0.10, 0.15, 0.20) along with its Rietveld refinement fitting using the above-mentioned space group through FullProf software is shown in **Figure 3.1.** Fitted HRXRD data confirms the presence of a single-phase system without any detectable impurity and structural instability. Crystallographic data and structural and fitting parameters obtained by refinement are listed in **Table 3.1,** which are in agreement with the values reported for $Dy_2Ti_2O_7$ [85].

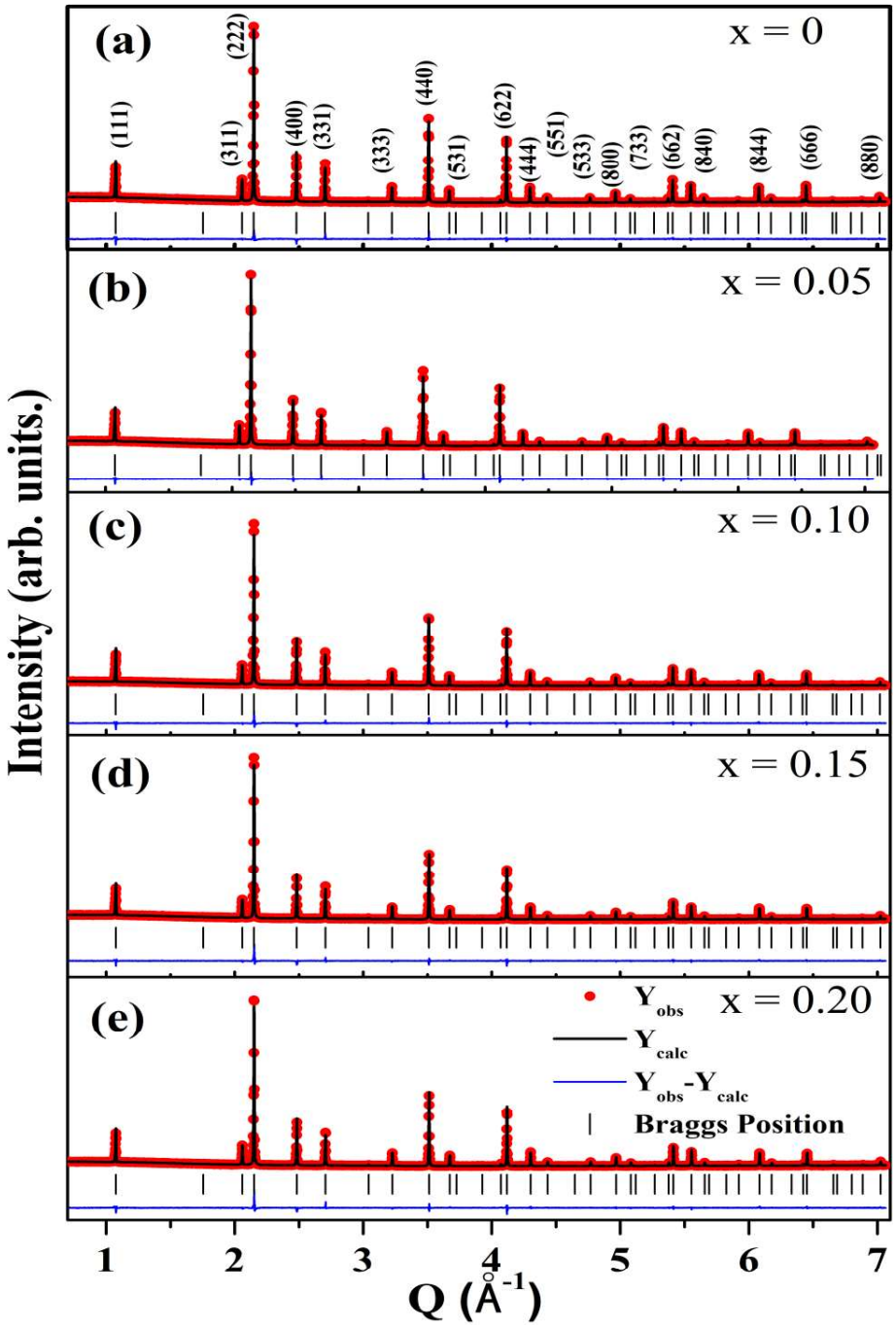

Figure 3.1 Room temperature high resolution x-ray diffraction (HRXRD) pattern of $Dy_2Ti_{2-x}Mn_xO_7$ (a) x = 0.00 (b) x = 0.05 (c) x = 0.10 (d) x = 0.15 (e) x = 0.20.

Table 3.1 Structural parameters including lattice parameters, bond length and bond angle obtained from Rietveld refinement of high-resolution x-ray diffraction data of $Dy_2Ti_{2-x}Mn_xO_7$.

Compound	Experimental lattice parameter (Å)	Bond Length (Å)				Bond Angle (°)		
$Dy_2Ti_{2-x}Mn_xO_7$		Dy-O1	Dy-O2	Ti-O	Dy-Dy	O1-Dy-O2	O1-Dy-O1	O1-Ti-O1
x = 0	10.1293(5)	2.5210(3)	2.1931(0)	1.9443(2)	3.5813(0)	80.01(7)	62.95(4)	85.21(2)
x = 0.05	10.1285(6)	2.5250(3)	2.1929(0)	1.9418(2)	3.5809(3)	80.11(7)	62.89(4)	85.44(2)
x = 0.10	10.1268(6)	2.5370(3)	2.1923(0)	1.9347(2)	3.5800(3)	80.38(7)	62.73(4)	86.07(2)
x = 0.15	10.1214(6)	2.5350(3)	2.1913(0)	1.9342(2)	3.5784(3)	80.37(7)	62.74(4)	86.04(2)
x = 0.20	10.1182(4)	2.5280(3)	2.1906(0)	1.9367(2)	3.5773(0)	80.24(7)	62.82(4)	85.73(2)

3.2.1 Role of Mn substitution on the structure

Substituting the smaller ionic radii element Mn at the Ti site results in the shrinkage in the lattice constant; values are given in **Table 3.1.**

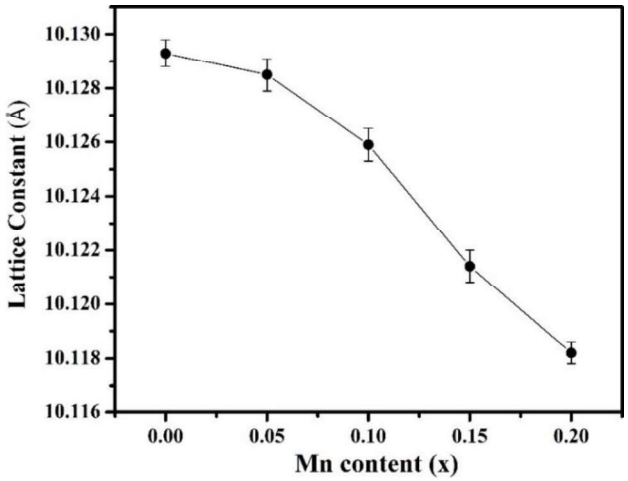

Figure 3.2 Variation of lattice parameter with x for $Dy_2Ti_{2-x}Mn_xO_7$ (x = 0, 0.05, 0.10, 0.15 0.20)

The sequential reduction in lattice parameter (obtained from Rietveld refinement) is shown pictorially in **Figure 3.2.** Shrinkage is further confirmed through the shift of prominent (311) and (222) hkl peaks towards the higher Q ($Å^{-1}$) value side with an increase in the percentage of Mn inclusion, as shown in **Figure 3.3.**

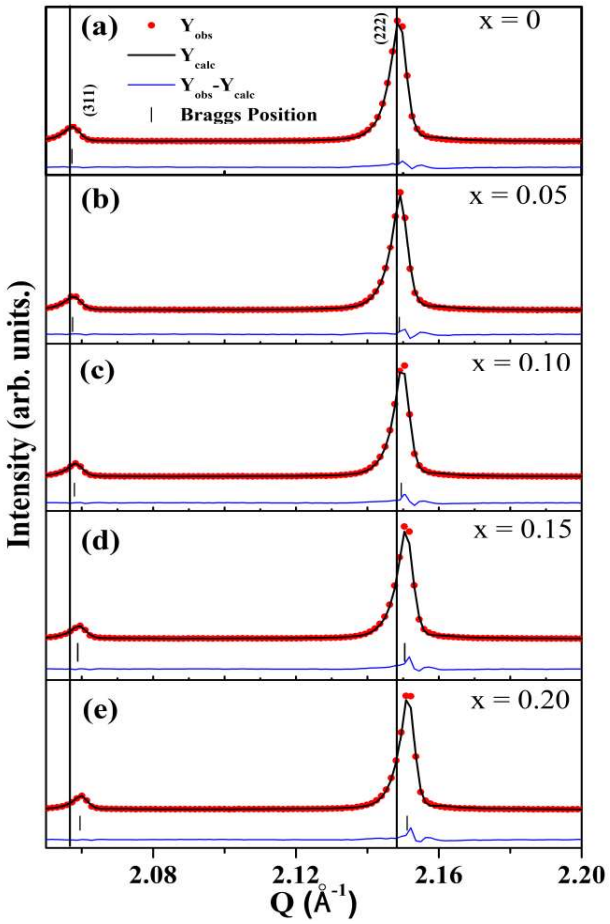

Figure 3.3 Room temperature high resolution x-ray diffraction data of $Dy_2Ti_{2-x}Mn_xO_7$ showing the shift of (311) and (222) peak towards higher Q value with increase in Mn inclusion for (a) x = 0 (b) x = 0.05 (c) x = 0.10 (d) x = 0.15 (e) x = 0.20.

3.3 Magnetic Properties

3.3.1 Temperature-dependent magnetization

In a disordered magnetic system, both dc and ac magnetization behaviour are studied to determine the exact nature of magnetic ordering. **Figure 3.4** depicts the temperature dependence of dc magnetization for $Dy_2Ti_{2-x}Mn_xO_7$ (x = 0, 0.05, 0.10, 0.15, 0.20) sample measured at 100 Oe and 1000 Oe in the temperature range from 2K to 200K using the zero-field cooling (ZFC) and field cooling (FC) protocol. In the recorded temperature range, there is no difference in the ZFC and FC curves for x = 0, 0.05, 0.10. However, the ZFC and FC curves bifurcate at lower temperatures, around 3 K for x = 0.15 and x = 0.20 (see **Figure 3.5**). For the purpose of comparison, we plotted the dc susceptibility for $Dy_2Ti_2O_7$ and the compound with maximum substitution, i.e., $Dy_2Ti_{1.8}Mn_{0.2}O_7$, in **Figure 3.6. Figure 3.6(a)** shows zero-field cooled (ZFC) and field-cooled (FC) magnetization data for $Dy_2Ti_2O_7$. There is no difference in ZFC and FC curves in the measured temperature range, suggesting no magnetic ordering and the absence of any transition down to 2 K, as reported earlier [85]. In contrast to the magnetic behaviour of $Dy_2Ti_2O_7$, $Dy_2Ti_{1.8}Mn_{0.2}O_7$ shows clear bifurcation in the ZFC and FC dc magnetic susceptibility at a temperature around 3.8 K, termed as T_{irr}, for the measurements taken at an applied field of 100 Oe as shown in (Figure 3.6 (a)). This irreversibility temperature shifts slightly towards the lower temperature side with an increase of the applied magnetic field of the measurement. Such irreversibility in ZFC and FC measurements and its behaviour with the increasing field indicates the spin states to be spin glass, cluster glasses or Griffiths-phase like [36], [86].

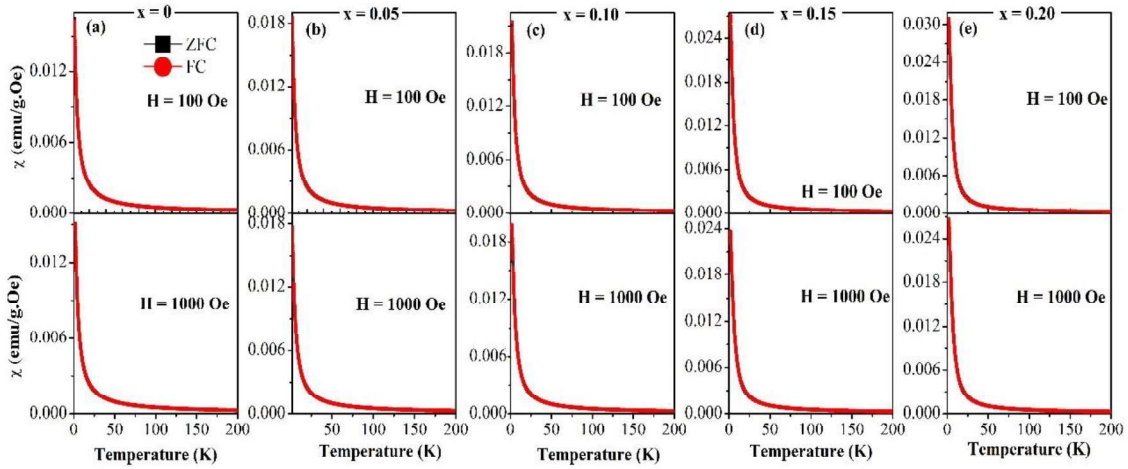

Figure 3.4 Temperature dependence of dc susceptibility for $Dy_2Ti_{2-x}Mn_xO_7$ (a) x = 0.00 (b) x = 0.05 (c) x = 0.10 (d) x = 0.15 (e) x = 0.20 at an applied magnetic field of 100 and 1000 Oe

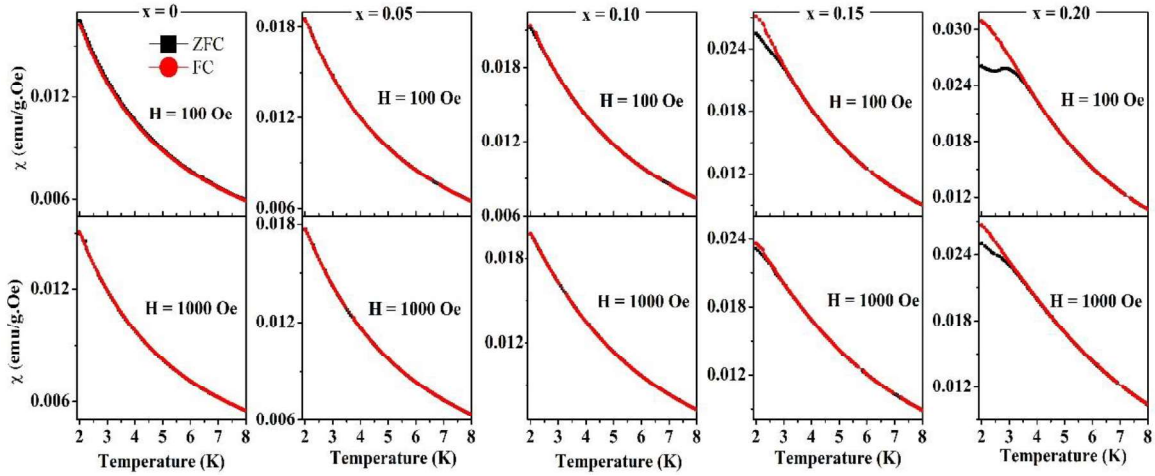

Figure 3.5 Temperature dependence of dc susceptibility for $Dy_2Ti_{2-x}Mn_xO_7$ (x= 0, 0.05, 0.10, 0.15, 0.20) at an applied magnetic field of 100 and 1000 Oe

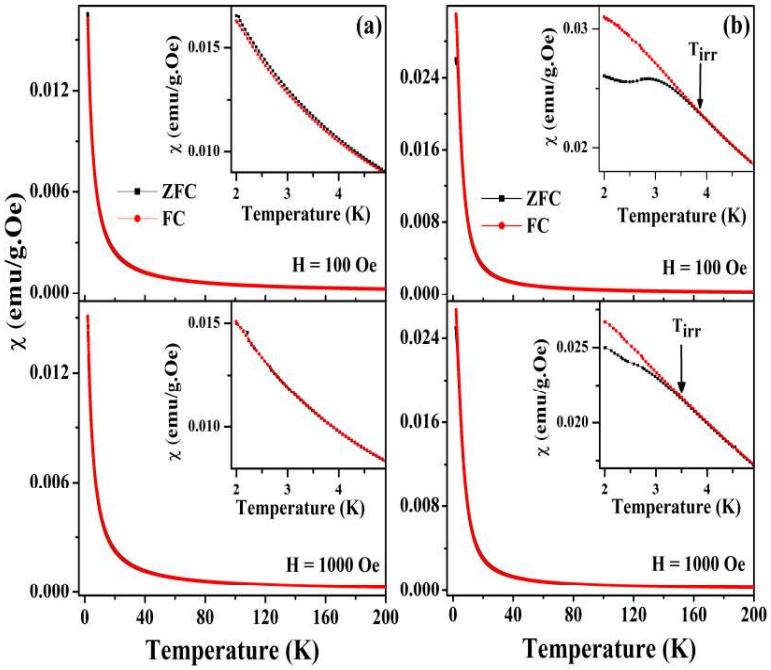

Figure 3.6 Temperature dependence of dc susceptibility for (a) $Dy_2Ti_2O_7$ and (b) $Dy_2Ti_{1.8}Mn_{0.2}O_7$ at an applied magnetic field of 100 and 1000 Oe.

Figure 3.7 shows the inverse susceptibility χ^{-1}(T) plot for x = 0 and x = 0.2. The analysis of the inverse susceptibility $\chi^{-1}(T)$ plot for $Dy_2Ti_2O_7$ shows a small deviation from Curie-Weiss law below 30 K, as shown in **Figure 3.7(a)**. It has been shown that dominance of the crystal electric field in $Dy_2Ti_2O_7$ starts setting up at a temperature ~30K, which onset the magnetic ordering in these systems [87], [88]. The corresponding behaviour of inverse susceptibility $\chi^{-1}(T)$ for $Dy_2Ti_{1.8}Mn_{0.2}O_7$ is very different. The first observation is the onset temperature of the deviation from Curie-Weiss law at a much higher temperature, around 60 K, as shown in **Figure 3.7(b)**. The second observation is the dip in $\chi^{-1}(T)$ data and its dependence on the magnetic field, typical of GP-like behaviour. This deviation in $\chi^{-1}(T)$ shows gradual softening with increasing fields from 100 Oe to 1500 Oe, as shown in **Figure 3.7(c)** [89]–[94].

A GP-like regime has the basic characteristic of having finite-size clusters with ferromagnetically correlated spins above T_C, which can further be characterized by hysteresis in the magnetization vs temperature curves in zero field-cooled, field-cooled cooling and field-cooled warming data.

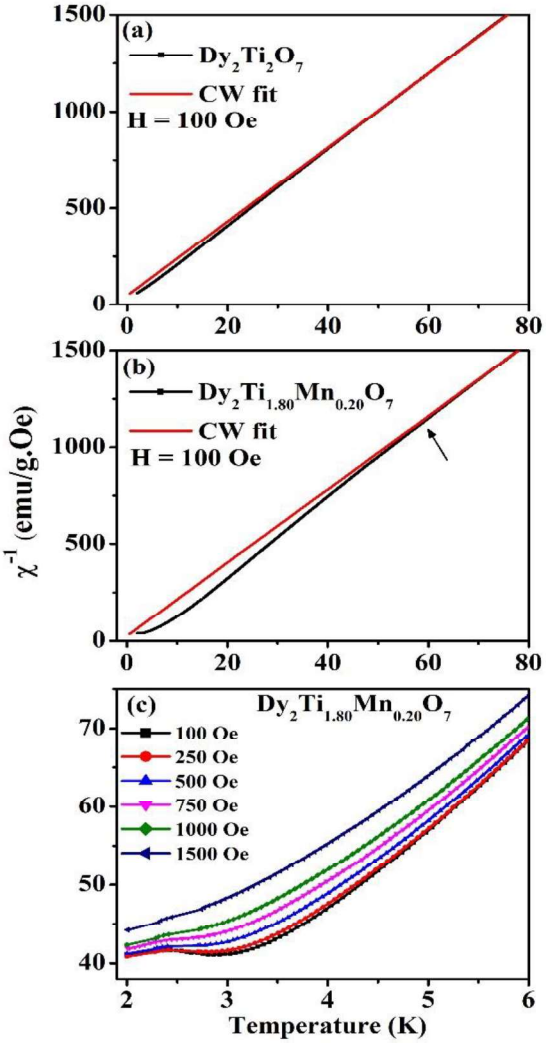

Figure 3.7 Curie-Weiss fit of inverse susceptibility χ^{-1}(T) plot for (a) $Dy_2Ti_2O_7$ and (b) $Dy_2Ti_{1.8}Mn_{0.2}O_7$ at an applied field of 100 Oe. (c) The inverse susceptibility χ^{-1}(T) plot for $Dy_2Ti_{1.8}Mn_{0.2}O_7$ at a different applied field.

Figure 3.8 shows the ZFC, FCC and FCW magnetization curve for x = 0.2 measured at an applied field of 100 Oe and 1000 Oe. The observed hysteresis in FCW and FCC curves confirms it exhibits inhomogeneous magnetism in a quantum critical regime below 5 K. This Weak hysteresis observed in the data collected on cooling and warming in FM/AFM phase can originate from the competition between the FM and AFM phases [95].

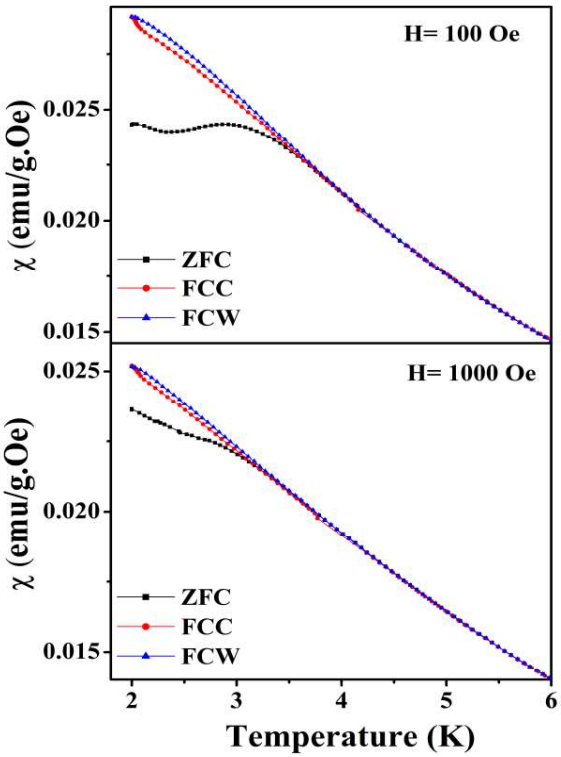

Figure 3.8 Zero field cooling (ZFC), field cool cooling (FCC) and warming (FCW) cycles of magnetization of $Dy_2Ti_{1.8}Mn_{0.2}O_7$ as a function of temperature at 100 Oe and 1000 Oe.

3.3.2 Field Dependent magnetization

Figure 3.9 shows the field dependence of the magnetization (M-H) curve, measured at 2 K for $Dy_2Ti_{2-x}Mn_xO_7$ (x = 0, 0.05, 0.10, 0.15, 0.20). The field was swept upto 50 kOe, down to

-50 kOe, and back up to 50 kOe to complete the loop. M_s value calculated from the M-H plot is 42.72 μ_B/unit cell in the case of $Dy_2Ti_2O_7$, which is consistent with the previously reported value [96], [97]. The M_s value increases to 44.78 μB/unit cell for compound with maximum substitution, i.e., x = 0.2. The obtained value is half of the actual magnetic moment due to the angular averaging in the powdered sample. The saturation value of magnetization (M_s) shows a slight increase for maximum substitution x = 0.2, indicating that inclusion does not measurably alter the system anisotropy [37]. The magnetization increases until an applied magnetic field of 20 kOe and then remains saturated to an applied field of 50 kOe.

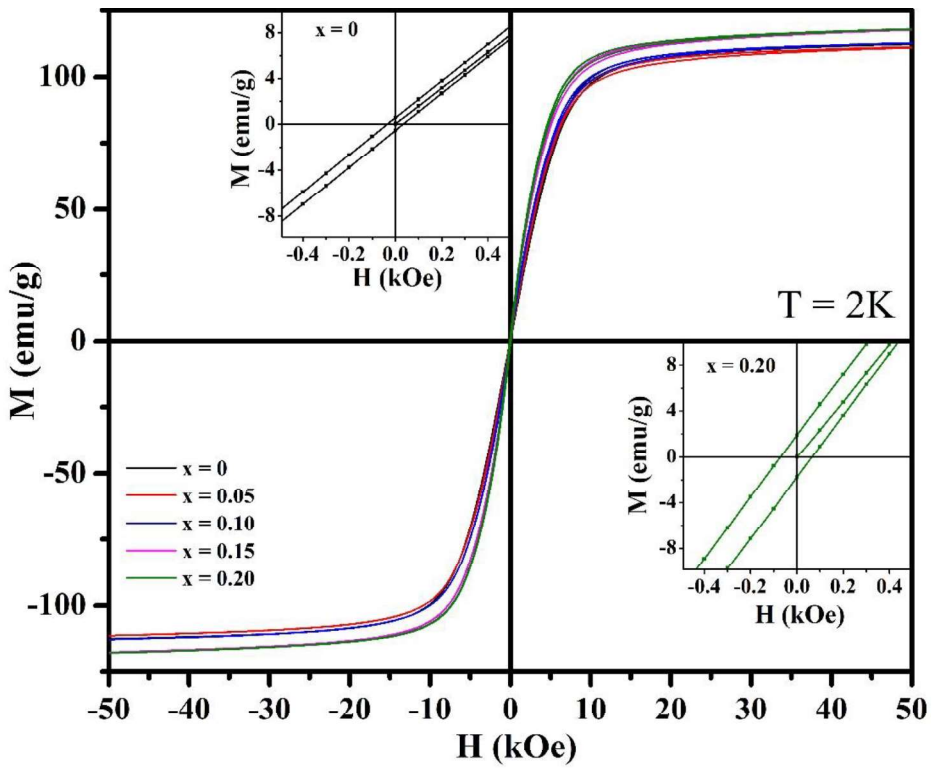

Figure 3.9 Magnetization as a function of Field (MH) curve for $Dy_2Ti_{2-x}Mn_xO_7$ (x = 0, 0.05, 0.10, 0.15, 0.20) at 2K for H (magnetic field) ranging from -50 to 50 kOe.

3.3.3 Temperature-dependent ac- susceptibility

With the dc magnetic susceptibility plot showing bifurcation for x = 0.15 and 0.20 at low temperature, we expect freezing out above this temperature in ac susceptibility data, so we performed a dynamic study of the system. **Figure 3.10** shows the real and imaginary part of field-dependent ac susceptibility measurements for $Dy_2Ti_{2-x}Mn_xO_7$ (x = 0, 0.05, 0.10, 0.15, 0.20) sample performed at 300 Hz. For more clarity, we plotted the ac susceptibility for $Dy_2Ti_2O_7$ and the compound with maximum substitution, i.e., $Dy_2Ti_{1.8}Mn_{0.2}O_7$, in a single figure at the various applied dc-bias fields as shown in **Figure 3.11.**

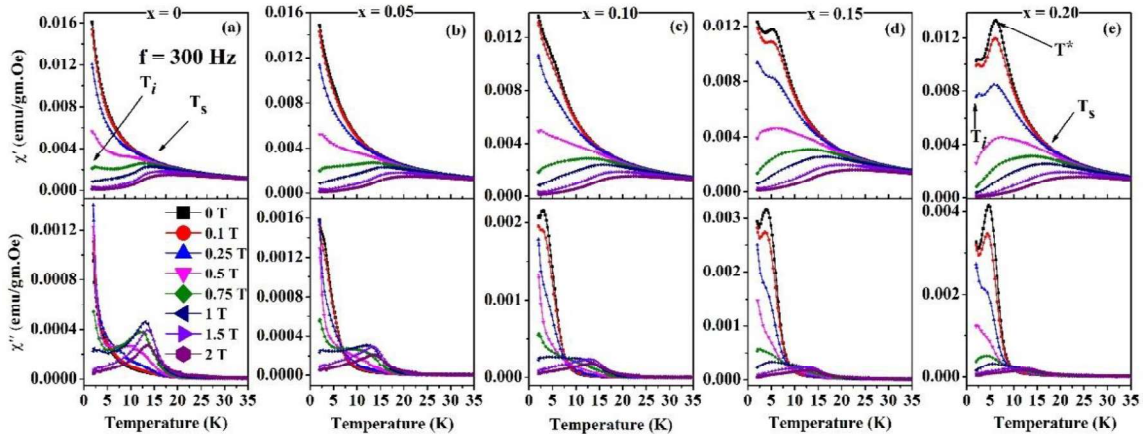

Figure 3.10 The real (upper panel) and imaginary part (lower panel) of ac susceptibility at different applied dc magnetic fields at frequency of 300 Hz for $Dy_2Ti_{2-x}Mn_xO_7$ (a) x = 0.00 (b) x = 0.05 (c) x = 0.10 (d) x = 0.15 (e) x = 0.20.

In the case of pure $Dy_2Ti_2O_7$ sample, we see that real part of ac susceptibility, $\chi'(T)$, is virtually identical to dc susceptibility in a low-temperature regime in the absence of applied dc bias field as depicted in **Figure 3.10(a)** or **Figure 3.11 (a)**, With an increase in the field beyond 0.25 T, we see the emergence of two relaxations, one corresponding to a single ion freezing

temperature (T_s) at around 15 K [37] and a spin ice state that emerges around 3 K (T_i) [98] in the real part of ac susceptibility $\chi'(T)$. We also observe a peak in $\chi''(T)$ corresponding to the maximum in $\chi'(T)$ as expected from the Kramer-Kronig relation [36], [53]. For spin-glasses and superparamagnets, the magnetic field suppresses the freezing temperature [99], [100]; however, the freezing at a higher temperature becomes more pronounced with an increase in the field, which is the characteristic of spin-ice. The single-ion freezing (T_s) shifts towards higher temperatures with an increased magnetic field. Such behaviour has been observed by Shi et al. in ac susceptibility measurements performed on a single crystal of $Dy_2Ti_2O_7$ [101].

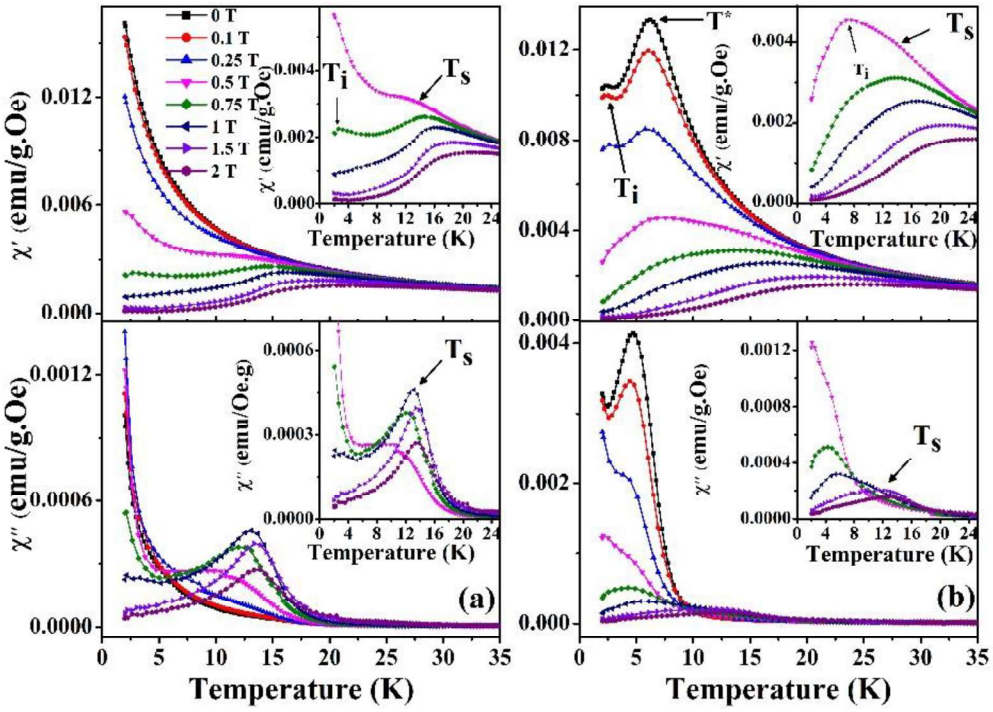

Figure 3.11 The real (upper panel) and imaginary part (lower panel) of ac susceptibility at different applied dc magnetic fields at frequency of 300 Hz for (a) $Dy_2Ti_2O_7$ (b) $Dy_2Ti_{1.8}Mn_{0.2}O_7$.

Similar is the case with x = 0.05 (**Figure 3.10 (b)**), but as we increase Mn dilution beyond x = 0.10, we see the emergence of a new peak around 5 K along with the appearance of spin ice freezing even in the absence of dc-bias field with further increasing the Mn concentration (for x = 0.20), peak becomes more pronounced (**Figure 3.10 (e)**). This suggests that the substitution of Mn at the Ti site alters the spin dynamics. In the case of x = 0.15 and x = 0.20, as shown in **Figure 3.10 (d, e)**, there appear two relaxations at a lower temperature near spin ice state even in the absence of dc field, the first one around 5 K (T*) and another one below T* at around 2.5 K (T_i) (**Figure 3.11**). T_i can be correlated to the low-temperature spin ice correlation freezing in $Dy_2Ti_2O_7$, which is studied in detail by Snyder et al. [36]. The anomaly peak T* is attributed to GP. The GP-like magnetic state has been inferred from magnetic frustration with Mn inclusion at the Ti site and alteration of crystal electric field at a low-temperature regime, indicating the altered magnetic landscape in the $Dy_2Ti_2O_7$ matrix [89]–[94]. The peak T* in can be related to Dy-Mn interactions and the possibility of alteration of the associated mean field. It is observed that the inclusion of Mn shifts the spin ice freezing state towards a higher temperature and gives a new relaxation peak (T*). Further, with the increase in the field, the single ion freezing (T_s) appears, and the one at the lowest temperature (T_i) disappears. T* broadens with the increase in the field.

To analyze the role of Mn inclusion, we plotted the ac susceptibility for $Dy_2Ti_2O_7$ and the compound with maximum substitution, i.e., $Dy_2Ti_{1.8}Mn_{0.2}O_7$ in a single figure at the various applied dc-bias fields as shown in **Figure 3.12**. **Figure 3.12(a)** shows spin ice freezing in $Dy_2Ti_{1.8}Mn_{0.2}O_7$ in the absence of dc bias, which is not observed in $Dy_2Ti_2O_7$, along with the appearance of a new peak T*. T* broadens as we increase the field to 0.5 T, as shown in **Figure 3.12 (b)**. As we increase the applied field to 0.75 T, the freezing at lower temperature

T_i disappears, and T* merges with T_s and gives a single hump-like feature for $Dy_2Ti_{1.8}Mn_{0.2}O_7$, as shown in **Figure 3.12(c)**. Further, increasing the field to 2 T, both $Dy_2Ti_2O_7$ and $Dy_2Ti_{1.8}Mn_{0.2}O_7$ show similar behaviour, as shown in **Figure 3.12 (f)**. This changed magnetic relaxation behaviour in $Dy_2Ti_{1.8}Mn_{0.2}O_7$ w.r.t. $Dy_2Ti_2O_7$ shows that the substitution of Mn alters the spin dynamics of the system at lower temperature regimes.

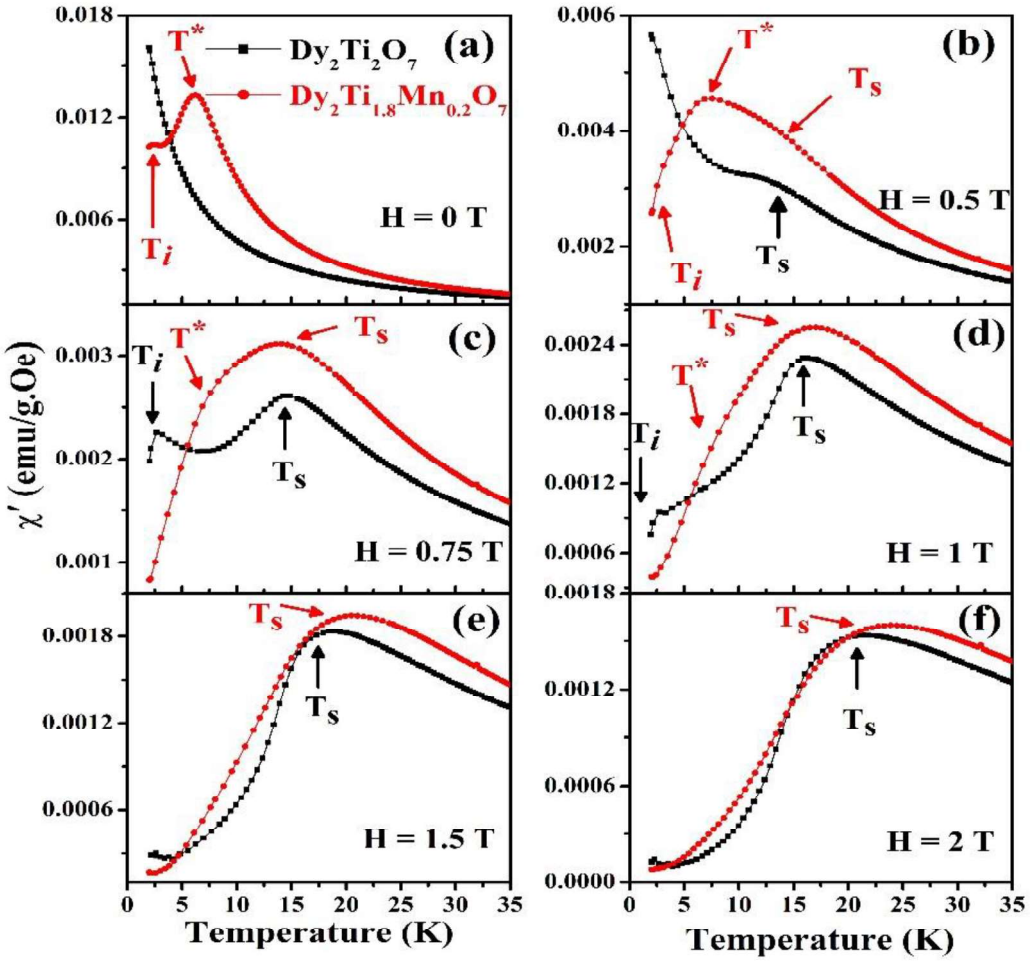

Figure 3.12 Temperature dependence of the real part of ac susceptibility measured at the 300 Hz frequency for $Dy_2Ti_2O_7$ and $Dy_2Ti_{1.8}Mn_{0.2}O_7$ at different DC bias fields (a) 0 T (b) 0.5 T (c) 0.75 T(d) 1 T (e) 1.5 T (f) 2 T

Further, to examine the nature of freezing phenomena, ac susceptibility data is collected in the vicinity of low temperature at varying frequencies ranging from 50 Hz to 700 Hz in the absence of applied dc fields. **Figure 3.13** shows the temperature-dependent ac susceptibility as a function of frequency for $Dy_2Ti_{2-x}Mn_xO_7$ (x = 0, 0.05, 0.10, 0.15, 0.20) sample series in the absence of an applied dc field.

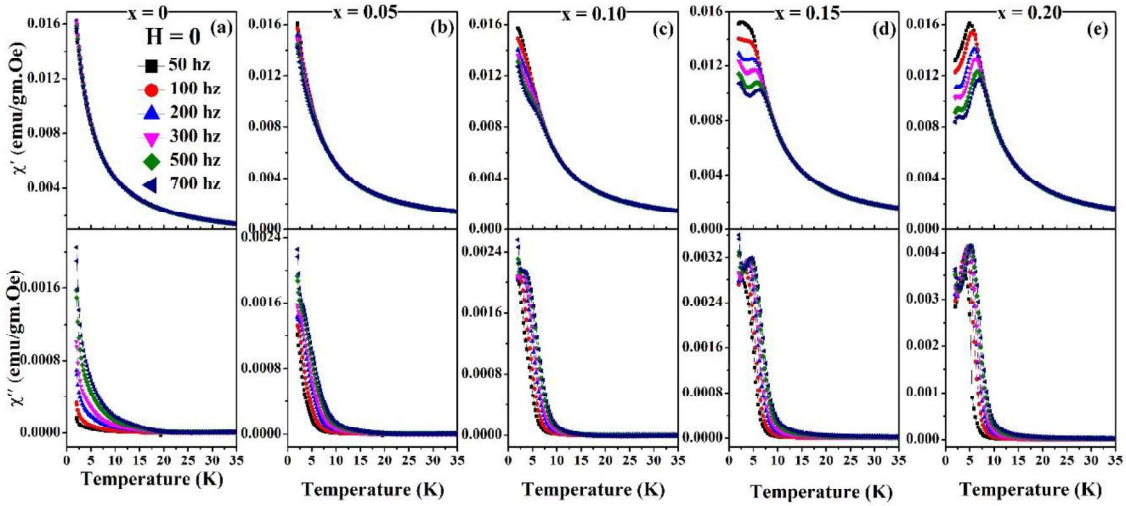

Figure 3.13 Frequency dependence of ac-susceptibility as a function of temperature for $Dy_2Ti_{2-x}Mn_xO_7$ (a) x = 0.00 (b) x = 0.05 (c) x = 0.10 (d) x = 0.15 (e) x = 0.20 at an applied field of 0 T.

The ac susceptibility for $Dy_2Ti_2O_7$ and the compound with maximum substitution i.e., $Dy_2Ti_{1.8}Mn_{0.2}O_7$, is depicted in **Figure 3.14**. The real part of ac susceptibility measurement $\chi'(T)$ shows canonical paramagnetic type behaviour for $Dy_2Ti_2O_7$ for all applied frequencies (f = 50, 100, 200, 300, 500, 700 Hz), corresponding to which there is a sharp increase in the imaginary part $\chi''(T)$ as shown in the lower panel as well. Whereas for $Dy_2Ti_{1.8}Mn_{0.2}O_7$, the lower temperature spin ice freezing, around 5 K (T*) shows strong frequency dependence. To

investigate the nature of (T*) as well as the spin dynamics in $Dy_2Ti_{1.8}Mn_{0.2}O_7$, we examined the frequency dependence of (T*) by fitting the data to an Arrhenius law given below

$$f = f_0 exp^{\frac{E_A}{K_B T}} \quad (3.1)$$

where E_A is the activation energy for spin fluctuations, K_B is the Boltzmann constant, and f_0 is a measure of the microscopic limiting frequency in the system . **Figure 3.15** shows the Arrhenius fit; the activation energy comes out to be 51.34 K for spin relaxation at T* in the case of $Dy_2Ti_{1.8}Mn_{0.2}O_7$ and $f_0 \sim 10^6$ Hz. Arrhenius law behaviour indicates that spin relaxation is thermally driven [38]. With Mn substitution, T* shifts towards the higher temperature side with an increase in frequency.

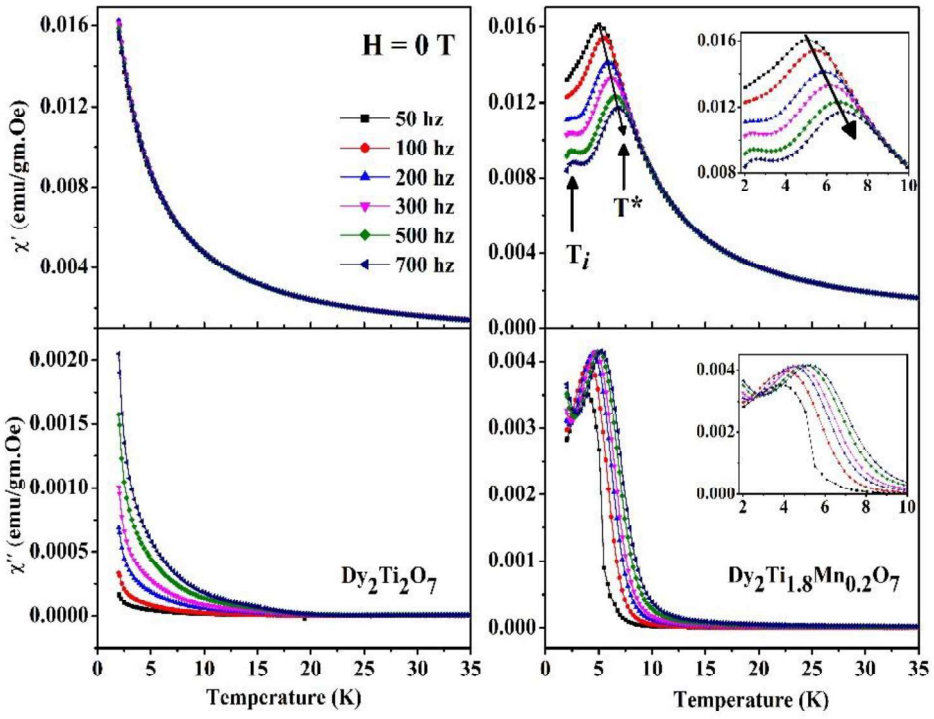

Figure 3.14 Frequency dependence of ac-susceptibility as a function of temperature for $Dy_2Ti_2O_7$ and $Dy_2Ti_{1.8}Mn_{0.2}O_7$ at an applied field of 0 T

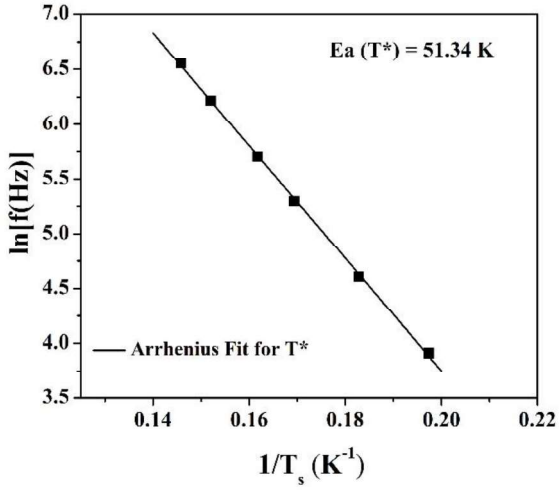

Figure 3.15 Arrhenius law fit of freezing temperature (T*) dependence on frequency for $Dy_2Ti_{1.8}Mn_{0.2}O_7$

3.3.4 Synchrotron x-ray diffraction

A small fraction of Mn inclusion significantly affects the crystal electric field of $Dy_2Ti_2O_7$. Furthermore, crystal field-phonon coupling may significantly affect spin dynamics. SXRD was performed from 140 K to 15 K at an interval of 10 K to establish the crystal field phonon coupling. **Figure 3.16** shows the selected low-temperature SXRD pattern for T = 140 K, 60 K, 30 K, and 15 K, along with its Rietveld refinement for $Dy_2Ti_2O_7$ and the compound with maximum substitution, i.e., for x = 0.2. Rietveld refinement of the synchrotron x-ray diffraction (SXRD) pattern was done using $Fd\bar{3}m$ space group through FULLPROF SUIT. The obtained value of the lattice constant for $Dy_2Ti_2O_7$ and $Dy_2Ti_{1.8}Mn_{0.2}O_7$ system at different temperature is listed in **Table 3.2**. The typical error in the lattice constant value for $Dy_2Ti_2O_7$ is of the order of 0.00015 and that for $Dy_2Ti_{1.8}Mn_{0.2}O_7$ is 0.00019.

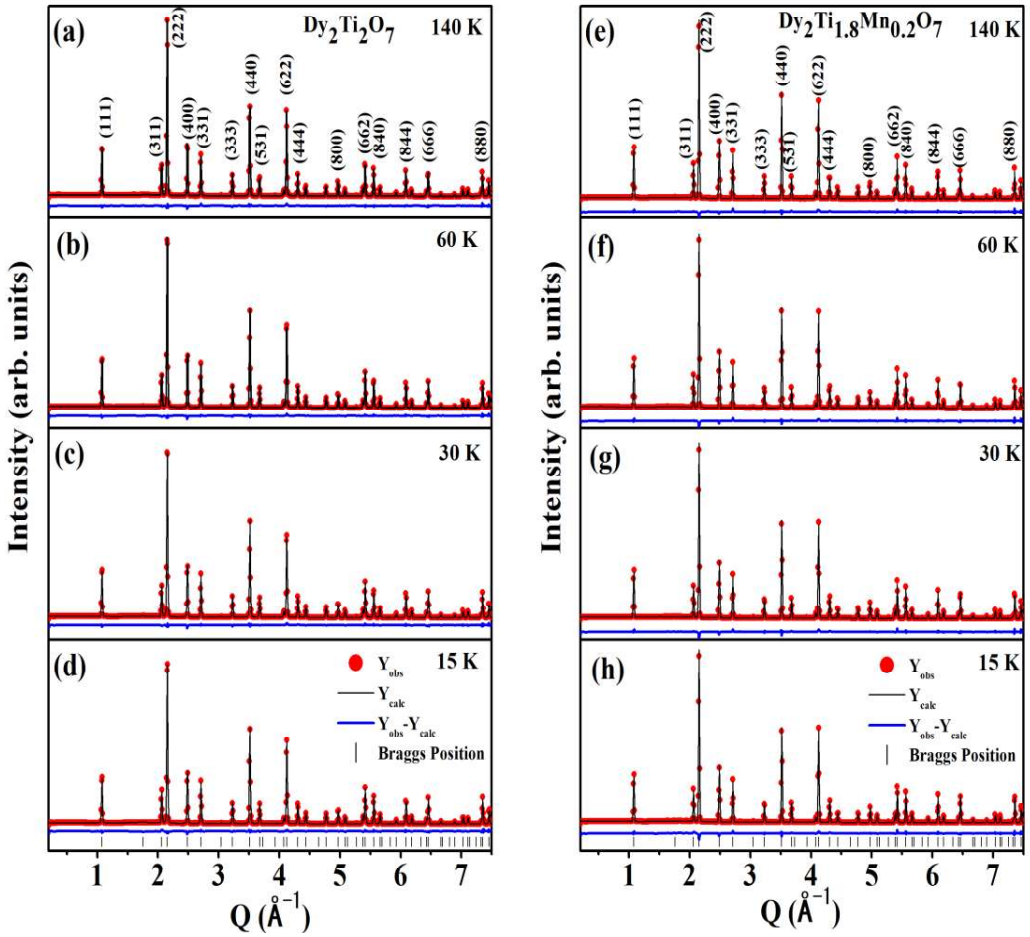

Figure 3.16 Rietveld refinement of low temperature synchrotron x-ray diffraction pattern of $Dy_2Ti_2O_7$ at (a) 140 K, (b) 60 K, (c) 30 K, (d) 15 K and $Dy_2Ti_{1.8}Mn_{0.2}O_7$ at (e) T = 140 K, (f) T = 60 K, (g) T = 30K and (h) T = 15K.

Temperature-dependent variation of lattice volume has been plotted. Debye Grüneisen equation has been fitted to extract the crystal field-induced change in the lattice volume. The equation is as follows:

$$V \cong V\,(T = 0) + \int_0^T \frac{\gamma C_v}{B}\, dT$$

$$\cong V\ (T=0) + \frac{9\gamma N k_B}{B} T \left(\frac{T}{\Theta_D}\right)^3 \int_0^{\Theta_D/T} \frac{e^x}{e^x - 1} dx \quad (3.2)$$

V (T=0), θ_D and $9\gamma Nk_B/B$ are fitting parameters; V(T = 0) represents the lattice volume at 0 K, θ_D is the Debye temperature, γ is the Grüneisen parameter, and B is the bulk modulus [102], [103]. Debye model contributes to thermal expansion due to anharmonic parts of lattice vibration.

Table 3.2 Obtained value of lattice constant for $Dy_2Ti_2O_7$ and $Dy_2Ti_{1.8}Mn_{0.2}O_7$ system at given temperature:

Temperature (K)	$Dy_2Ti_2O_7$	$Dy_2Ti_{1.8}Mn_{0.2}O_7$
	a (Å)	a (Å)
140	10.1193	10.1106
130	10.1188	10.1101
120	10.1183	10.1096
110	10.1177	10.1089
100	10.1170	10.1084
90	10.1164	10.1079
80	10.1162	10.1075
70	10.1158	10.1073
60	10.1150	10.1070
50	10.1147	10.1069
40	10.1145	10.1066
30	10.1144	10.1061
20	10.1133	10.1048
15	10.1131	10.1045

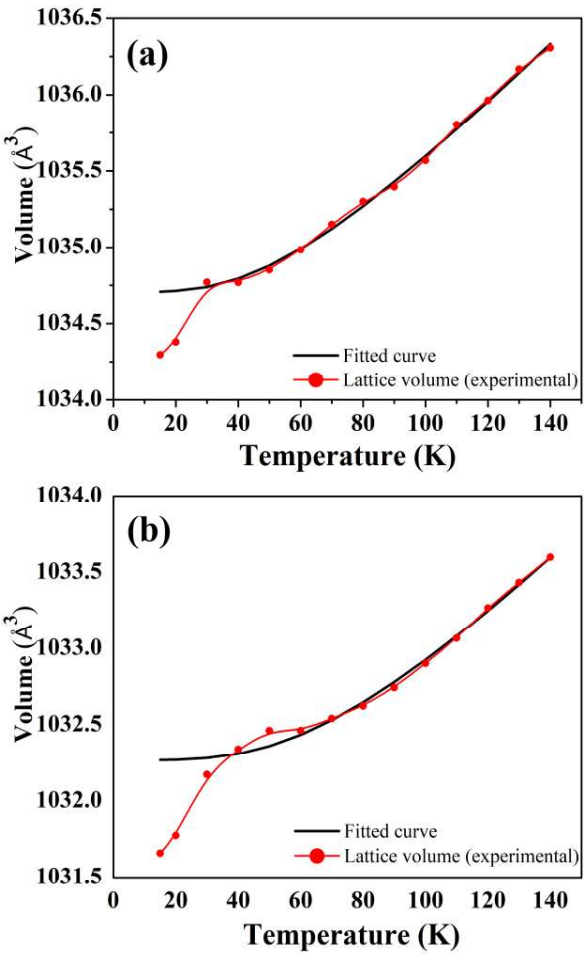

Figure 3.17 Temperature variations of unit cell parameters solid line (black) represents the fitted curve contribution of phonons by Debye Gruineisen, and solid circle (red) represents experimental lattice volume (a) $Dy_2Ti_2O_7$ and (b) $Dy_2Ti_{1.8}Mn_{0.2}O_7$.

As shown in **Figure 3.17(a)**, lattice volume decreases linearly till 30 K, below which it shows apparent deviation from Debye-Gruineisen fit, showing the dominance of crystal field at low temperature in case of $Dy_2Ti_2O_7$, but for $Dy_2Ti_{1.8}Mn_{0.2}O_7$ (**Figure 3.17(b)**), lattice volume decreases as per Debye equation till 70 K then it deviates and becomes constant again, it drops below 40 K which suggests that with Mn substitution crystal field prominence starts at higher

temperature (70 K). The obtained value of $V(T = 0)$, θ_D and $9\gamma Nk_B/B$, fitting parameters, are depicted in **Table 3.3**. It shows the enhancement in Debye temperature with Mn inclusion at the Ti site to $\theta_D = 290.6$ K for $Dy_2Ti_{1.8}Mn_{0.2}O_7$ compared to $\theta_D = 214.1$ K for $Dy_2Ti_2O_7$. Such an enhancement shows the increase in the crystal field energy dominance to set in at a higher temperature in the case of $Dy_2Ti_{1.8}Mn_{0.2}O_7$ at 70 K.

Table 3.3 The parameters V (T = 0), θ_D and $9\gamma Nk_B/B$ for $Dy_2Ti_2O_7$ and $Dy_2Ti_{1.8}Mn_{0.2}O_7$ were obtained by fitting Debye Function.

Compound	**$Dy_2Ti_2O_7$**	**$Dy_2Ti_{1.8}Mn_{0.2}O_7$**
V(T=0K) (Å^3)	1034.7	1032.3
Debye temperature, $\theta_D(K)$	214.1	290.6
$9\gamma Nk_B/B$ (Å^3 /K)	0.065	0.066

3.4 Conclusions

We have studied low-temperature magnetic ordering and spin dynamics for the polycrystalline compound $Dy_2Ti_{2-x}Mn_xO_7$ (x= 0, 0.05, 0.10, 0.15, 0.20). The sequential increase in the percentage inclusion of smaller ionic radii element Mn^{4+} at the Ti^{4+} site in $Dy_2Ti_2O_7$ decreases the lattice parameter Mn-O bond length and increases the O1-Ti-O1 or O1-Mn-O1 bond angle distortion in MnO_6 octahedron. With small Mn inclusion at the Ti site in $Dy_2Ti_2O_7$, we observe the bifurcation in FC and ZFC in dc susceptibility measurement. The temperature variation of inverse susceptibility $\chi^{-1}(T)$ and weak hysteresis observed in the data collected on cooling (FCC) and warming (FCW) in FM/AFM phase, evolving in $Dy_2Ti_{1.8}Mn_{0.2}O_7$ confirms the GP-like state. GP-like state is inferred from magnetic frustration with Mn inclusion at the Ti site. There is an emergence of a new relaxation feature around 5 K (T*) along with the enhancement of spin ice freezing (T_i) in ac susceptibility measurement even in the absence of

any dc magnetic field, which was not observed in the case of $Dy_2Ti_2O_7$. The spin relaxation at T* shows strong frequency dependence and Arrhenius fit shows that this spin relaxation is thermally driven. The peak T* can be related to Dy-Mn interactions and the modulation of the crystal electric field at low temperatures. The low-temperature Synchrotron x-ray diffraction study confirms the absence of structural phase transition in this system. Debye parameters are calculated by fitting Temperature-dependent variation of lattice volume using the Debye Gruineisen equation. It shows that crystal field energy dominance set in at higher temperatures in the case of Mn-substituted $Dy_2Ti_2O_7$. Such a small perturbation in the composition leads to magnetic ordering above the transition temperature. Nevertheless, the evolution of Griffiths phase behaviour is associated with the compositional inclusion of Mn at the Ti site in $Dy_2Ti_2O_7$ and the differences displayed in spin dynamics of $Dy_2Ti_{2-x}Mn_xO_7$. There are still considerable challenges to our current understanding of these strongly correlated systems. Further neutron experiments and theoretical calculations may help to fully understand the system.